Title

Human Cytomegalovirus IE2 Protein Disturbs Brain Development by the Dysregulation of Neural Stem Cell Maintenance and the Polarization of Migrating Neurons

Journal

Journal of Virology, 91(17)

ISSN

0022-538X

Authors

Han, Dasol
Byun, Sung-Hyun
Kim, Juwan
et al.

Publication Date

2017-09-01

DOI

10.1128/jvi.00799-17

Peer reviewed

AMERICAN SOCIETY FOR MICROBIOLOGY | Journal of Virology®

PATHOGENESIS AND IMMUNITY

Human Cytomegalovirus IE2 Protein Disturbs Brain Development by the Dysregulation of Neural Stem Cell Maintenance and the Polarization of Migrating Neurons

Dasol Han,[a] Sung-Hyun Byun,[a] Juwan Kim,[a] Mookwang Kwon,[a] Samuel J. Pleasure,[b] Jin-Hyun Ahn,[c] Keejung Yoon[a]

College of Biotechnology and Bioengineering, Sungkyunkwan University, Suwon, Gyeonggi-do, Republic of Korea[a]; Department of Neurology, University of California San Francisco, San Francisco, California, USA[b]; Department of Molecular Cell Biology, Samsung Biomedical Research Institute, Sungkyunkwan University School of Medicine, Suwon, Gyeonggi-do, Republic of Korea[c]

ABSTRACT Despite the high incidence of severe defects in the central nervous system caused by human cytomegalovirus (HCMV) congenital infection, the mechanism of HCMV neuropathogenesis and the roles of individual viral genes have not yet been fully determined. In this study, we show that the immediate-early 2 (IE2) protein may play a key role in HCMV-caused neurodevelopmental disorders. IE2-transduced neural progenitor cells gave rise to neurospheres with a lower frequency and produced smaller neurospheres than control cells *in vitro*, indicating reduction of self-renewal and expansion of neural progenitors by IE2. At 2 days after *in utero* electroporation into the ventricle of the developing brain, a dramatically lower percentage of IE2-expressing cells was detected in the ventricular zone (VZ) and cortical plate (CP) compared to control cells, suggesting that IE2 concurrently dysregulates neural stem cell maintenance in the VZ and neuronal migration to the CP. In addition, most IE2$^+$ cells in the lower intermediate zone either showed multipolar morphology with short neurites or possessed nonradially oriented processes, whereas control cells had long, radially oriented monopolar or bipolar neurites. IE2$^+$ callosal axons also failed to cross the midline to form the corpus callosum. Furthermore, we provide molecular evidence that the cell cycle arrest and DNA binding activities of IE2 appear to be responsible for the increased neural stem cell exit from the VZ and cortical migrational defects, respectively. Collectively, our results demonstrate that IE2 disrupts the orderly process of brain development in a stepwise manner to further our understanding of neurodevelopmental HCMV pathogenesis.

IMPORTANCE HCMV brain pathogenesis has been studied in limited experimental settings, such as *in vitro* HCMV infection of neural progenitor cells or *in vivo* murine CMV infection of the mouse brain. Here, we show that IE2 is a pivotal factor that contributes to HCMV-induced abnormalities in the context of the embryonic brain using an *in utero* gene transfer tool. Surprisingly, IE2, but not HCMV IE1 or murine CMV ie3, interferes pleiotropically with key neurodevelopmental processes, including neural stem cell regulation, proper positioning of migrating neurons, and the callosal axon projections important for communication between the hemispheres. Our data suggest that the wide spectrum of clinical outcomes, ranging from mental retardation to microcephaly, caused by congenital HCMV infection can be sufficiently explained in terms of IE2 action alone.

KEYWORDS brain development, HCMV, neural stem cells

Received 12 May 2017 **Accepted** 8 June 2017

Accepted manuscript posted online 14 June 2017

Citation Han D, Byun S-H, Kim J, Kwon M, Pleasure SJ, Ahn J-H, Yoon K. 2017. Human cytomegalovirus IE2 protein disturbs brain development by the dysregulation of neural stem cell maintenance and the polarization of migrating neurons. J Virol 91:e00799-17. https://doi.org/10.1128/JVI.00799-17.

Editor Jae U. Jung, University of Southern California

Address correspondence to Keejung Yoon, keejung@skku.edu.

Human cytomegalovirus (HCMV) is a member of the betaherpesviruses that infect most human populations in the world and establishes a lifelong infection, with cycles of repeating latency and reactivation (1). Although HCMV infection is mostly asymptomatic or subclinical in immunocompetent individuals, it can cause morbidity and mortality in immunocompromised patients (1). Because of widespread infection in human populations, the absence of an effective vaccine, and easy mother-to-fetus viral transmission, HCMV is the most common cause of congenital infections (2) and also the leading viral cause of birth defects, affecting 0.25% to 2% of newborn infants worldwide (3).

Up to 10% of congenitally HCMV-infected newborns have overt clinical manifestations at birth, including microcephaly, thrombocytopenia, jaundice, hepatomegaly, and occasionally life-threatening systemic complications (4). The remaining infected infants have no clinical manifestations at birth, but some will still have defects in brain functions, such as mental retardation, visual and hearing disorders, seizures, and epilepsy (3, 5, 6). Infections during early pregnancy generally lead to more severe clinical manifestations in newborns (5).

For proper brain development, neural stem cell number and expansion must be closely regulated. Embryonic neural stem cells are maintained in the ventricular zone (VZ), and as brain development proceeds, they differentiate into cells with neuronal lineage commitment and migrate away from the VZ to the outer surface of the brain to form cortical lamination (7). The failure of precise regulation of neural stem cell proliferation and differentiation causes developmental abnormalities in the brain such as microcephaly and mental retardation (8).

HCMV brain pathogenesis has been studied mainly in cultured neural progenitor cells *in vitro* because of the lack of an appropriate animal model due to the strict species-specific tropism of HCMV that only allows virus replication in cells of human origin (9). To circumvent this limitation, an animal model using murine CMV (MCMV) infection of the mouse brain has been used to provide insight into CMV pathogenesis in the central nervous system (CNS) (10, 11). However, since MCMV differs considerably from HCMV with respect to immediate-early (IE) gene organization, overall nucleotide sequence, and corresponding biological properties (12), there have been limitations in extrapolating data from the experimental animal MCMV model to HCMV pathogenesis in the human brain.

To better understand the pathogenesis of viruses with a large and complicated genome like HCMV, in-depth studies analyzing cellular and molecular changes at a single-gene level as well as the whole-virus level are required. Considering that gene function studies inducing expression of a viral gene of interest by vectors circumvent the issue of host cell tropism, it is surprising that few attempts, to our knowledge, have been made to assess the effect of individual HCMV genes *in vivo* using an animal model.

In this study, we show that expression of the HCMV immediate-early 2 (IE2) protein has a profound negative impact on the proliferation and self-renewal capacity of neural progenitor cells *in vitro*. Expression of HCMV IE2 protein also induces premature differentiation of neural stem cells and accumulation of nonfunctional immature neurons during brain development *in vivo*. Our study provides insight into the molecular pathogenesis mechanisms by which a complex virus, HCMV, disturbs the development of the most complex organ, the brain.

RESULTS

Expression of HCMV IE2, but not IE1, impairs the self-renewal and proliferation of neural progenitor cells *in vitro*. For efficient gene delivery into primary neural progenitor cells, IE1 and IE2 genes were cloned into the retroviral vector MSIG (13) (Fig. 1A). MSIG contains an internal ribosome entry site (IRES) sequence for bicistronic expression of IE1 or IE2 and green fluorescent protein (GFP) as a reporter. Western blotting (Fig. 1B) and immunofluorescence (Fig. 1C) showed that the constructs expressed proteins of the expected sizes for each IE protein and GFP in target cells.

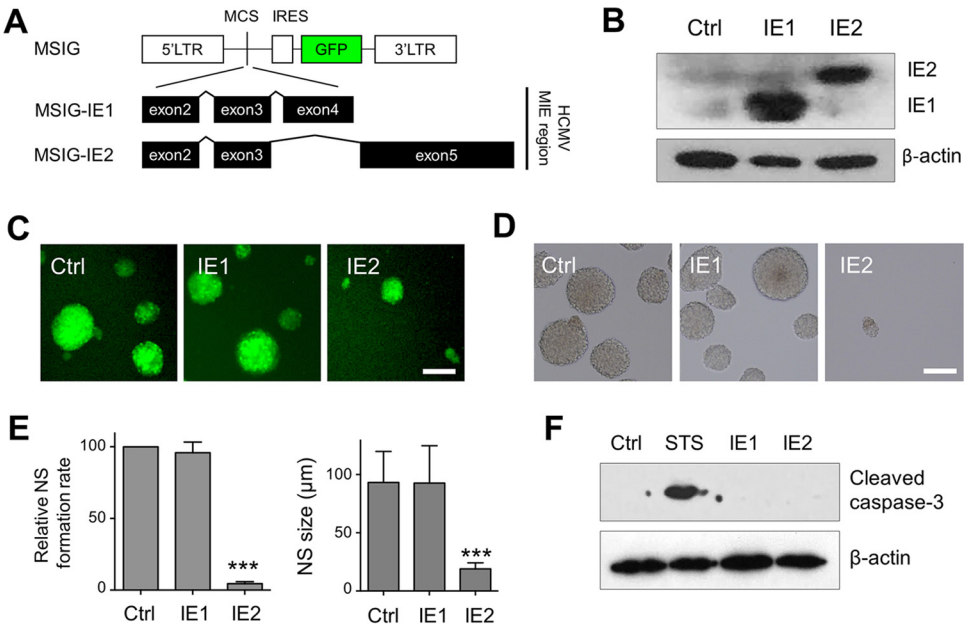

FIG 1 HCMV IE2 expression, but not IE1 expression, negatively regulates neural stem cells *in vitro*. (A) Schematic representation of the retroviral vector used in this study. The retroviral vector MSIG, which bicistronically expresses HCMV IE and GFP, was used to transduce primary embryonic neural progenitor cells. MSIG expressing only GFP was used as a control. IRES, internal ribosome entry site; LTR, long terminal repeat; MCS, multicloning site; MIE, major immediate early. Expression of IE1/2 and GFP in transduced target cells was confirmed by Western blotting using an anti-IE antibody (B) and fluorescence microscopy (C), respectively. (D) Effect of IE1 and IE2 on neurosphere formation. E14.5 primary neural progenitors transduced with each retroviral vector were cultured for 7 days in serum-free medium supplemented with B27/N2 and FGF2. (E) Quantification of neurosphere frequency and size from panel D. (F) Test for possible cytotoxic effects of IE proteins. Cell lysates from primary neural progenitors transduced with each retroviral vector and cultured for 2 days were tested for cleaved caspase-3 generation by Western blotting. Staurosporine (STS; 2 μM; 8 h of incubation) was used as a positive control. Scale bars, 100 μm. Error bars represent standard deviations (SD). Student's *t* test was used to determine statistical significance. ***, $P < 0.001$; $n \geq 3$.

To test the effect of IE proteins on embryonic neural progenitor cells *in vitro*, we began with neurosphere cultures using mouse embryonic day 14.5 (E14.5) neural progenitors. The neurosphere assay is a clonal cell survival assay based on the ability of a single neural stem cell to grow into a colony (neurosphere) in defined stem cell media (14). By measuring neurosphere frequency and size, the effects of a gene of interest on self-renewal and proliferative activities, respectively, can be determined for stem cells. As shown in Fig. 1D and E, IE2-transduced cells gave rise to far lower frequencies of neurospheres and smaller neurospheres than control cells, indicating reduction of self-renewal and cell proliferative capabilities upon IE2 expression, whereas IE1 expression did not appear to have any deleterious effects on neurosphere formation. To rule out the possibility that IE2 exerts its negative influences on neural progenitor cells through cytotoxic activity, we performed Western blotting to detect the active form of caspase-3, a marker for apoptosis, and found that cleaved caspase-3 was undetectable in IE2-transduced neural progenitor cells (Fig. 1F). Taken together, these results indicate that IE2 negatively regulates neural stem cell characteristics *in vitro*, and these observations were not due to increased cell death.

IE2 negatively acts on multiple steps of brain development *in vivo*. We next tested the effects of IE2 expression on neural stem cells *in vivo*. Neural stem cells reside and proliferate in the VZ throughout brain development, and cells undergoing differentiation into neurons migrate away from the VZ to cross the intermediate zone (IZ) and reach the cortical plate (CP). For *in vivo* transgene expression in the developing brain, IE2-expressing plasmid DNA was introduced into the telencephalic ventricle of E13.5 embryos by *in utero* electroporation (Fig. 2A), and the outcomes of IE2 expression were analyzed at E15.5. Initially, only cells lining the ventricles (thus, mostly neural stem

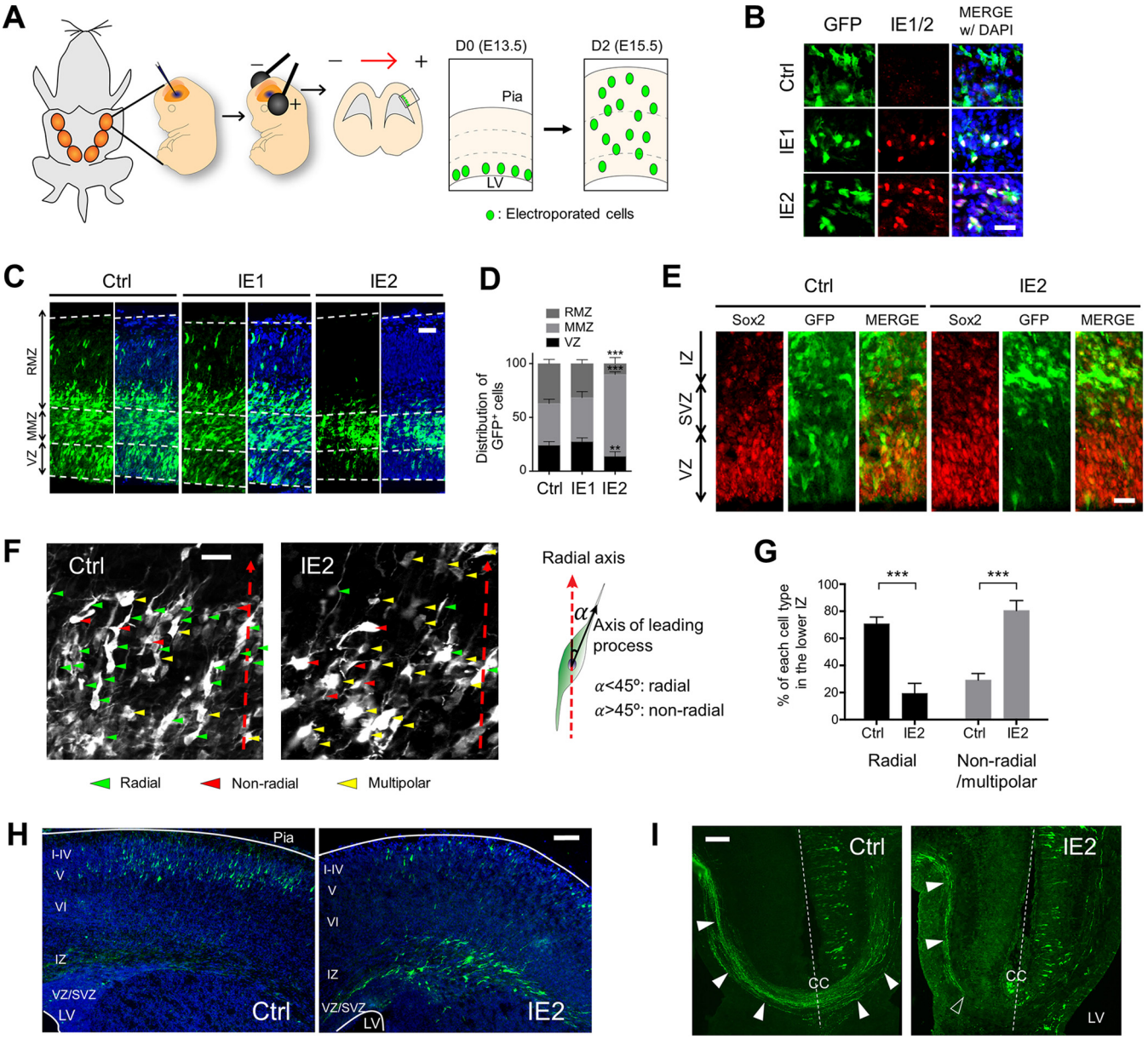

FIG 2 HCMV IE2 expression disturbs cortical brain development *in vivo*. (A) Schematic of gene delivery into the embryonic brain through *in utero* electroporation of plasmid DNA and assessment of the neurodevelopment-modulating activity of a gene of interest by determining the transgene-expressing cell positions in the cortical layers. Initially, only neural stem cells lining the VZ are electroporated, and as development proceeds, they give rise to neural stem cells that reside in the VZ or neurons that migrate up to the pial surface. (B) IE expression in the brains at 2 days postelectroporation was confirmed by immunostaining using anti-GFP (reporter gene; green) and anti-IE1/2 (red) primary antibodies as well as Alexa Fluor 488- and 555-conjugated secondary antibodies. IE2-expressing cells in E15.5 (C) or E18.5 (H and I) embryonic brains that were electroporated at E13.5 were immunolabeled using anti-GFP primary and Alexa 488-conjugated secondary antibodies. For panel C, GFP immunofluorescence merged with DAPI-counterstained images are shown on the right. (D) Quantification of GFP^+ cell positions from panel C. (E) Double immunolabeling of E15.5 brain sections electroporated with IE2-expressing plasmid at E13.5 using anti-GFP (green) and anti-Sox2 (red) primary antibodies. (F) The shapes of GFP^+ electroporated cells in E15.5 cortices at the transition between MMZ and RMZ. The dotted red lines indicate the direction of radial migration. Radial cells were defined as cells with a leading process with a deviation angle of less than 45° relative to the normal radial migration direction. (G) Quantification of cell shapes shown in panel F. (I) Examination of callosal axon trajectory (closed arrowheads) using immunolabeling of GFP at E18.5. The dotted lines indicate the midline, and an open arrowhead indicates where $IE2^+$ callosal axons stop projection. VZ, ventricular zone; SVZ, subventricular zone; IZ, intermediate zone; CP, cortical plate; MMZ, multipolar morphology zone; RMZ, radial morphology zone; CC, corpus callosum; LV, lateral ventricle. Scale bars were 20 μm (B, E, and F), 50 μm (C), and 100 μm (H and I). Error bars represent SD. Student's *t* test was used to determine statistical significance. **, $P < 0.01$; ***, $P < 0.001$; $n \geq 3$.

cells) are transfected by electroporation, and after a certain period of time, the distribution of gene-transferred cells in the cortical laminar layers are visualized by immunofluorescence against the GFP reporter protein to analyze the differentiation pattern of transgene-expressing cells. IE and GFP expression levels after *in utero*

electroporation were verified by immunofluorescence using anti-IE1/2 and anti-GFP antibodies (Fig. 2B). As shown in Fig. 2C and D, IE2 expression resulted in significant changes in cell localization in the embryonic brain. At 2 days postelectroporation, a dramatically higher fraction of IE2-transfected cells was detected in the multipolar morphology zone (MMZ) than in control cells. Far lower percentages of IE2-expressing cells in the VZ and CP indicate that IE2 dysregulates neural stem cell maintenance as well as neuronal migration and maturation. Enhanced cell exit from the VZ upon IE2 expression was further confirmed by immunostaining using an anti-Sox2 antibody (Fig. 2E). The delay in migration of IE2-expressing cells toward the pial surface was still obvious at E18.5 and thus was presumed to be maintained throughout brain development (Fig. 2H). The presence of a large number of IE2-expressing cells in the transfected brain up to 5 days postelectroporation also provides evidence for the cytotoxicity-independent dysregulation of brain development by IE2.

In addition, there was a prominent difference in cellular morphology between $IE2^+$ and control cells in the boundary region between the MMZ and radial morphology zone (RMZ), where multipolar-to-bipolar transition occurs. Control cells had long, radially oriented monopolar or bipolar neurons, whereas most $IE2^+$ cells either showed multipolar morphology with short neurites or possessed a leading process deviating from the normal radial migrating direction (Fig. 2F). To quantify these observations, the deviation angle of the leading process relative to the normal radial migration direction was measured, and cells with a deviation angle of less than 45° were defined as radial cells and the others as nonradial cells (Fig. 2G).

The neocortical hemispheres are connected via a large axon bundle, the corpus callosum. This connection is achieved by the orderly projection of axons over long distances from one side of the cortex to the equivalent contralateral cortical area (15). As shown in Fig. 2I, callosal axons of IE2-expressing cells failed to project into the topographically equivalent locations in the contralateral brain area at E18.5. Taken together, these results indicate that IE2 disrupts multiple processes of brain development, including neural stem cell maintenance in the VZ, migrating neuronal polarization, radial migration, and callosal axon projection linking the two hemispheres.

Expression of MCMV ie3, the MCMV homolog of HCMV IE2, has no detrimental effects on neural stem regulation. Because of the high level of conservation between HCMV IE2 and MCMV ie3 with regard to amino acid sequence, gene structure, and protein functions (16), we tested if expression of MCMV ie3 could exert negative effects similar to those of HCMV IE2 in neural stem cell regulation. Interestingly, MCMV ie3 behaved like the negative control both *in vitro* and *in vivo*; MCMV ie3 expression appeared to have no inhibitory effects on the formation rate and size of neurospheres (Fig. 3B and C). The cell distribution pattern in the developing brain also was not affected by ie3 expression induced by *in utero* electroporation (Fig. 3E and F). Taken together, these results indicate that despite its similarity to HCMV IE2, MCMV ie3 is not associated with neural stem cell misregulation.

IE2 expression dysregulates neural progenitor cells *in vitro* through cell cycle-inhibitory and DNA binding activities. To address how IE2 perturbs neural stem cell properties, we generated two functional mutant IE2 genes by site-directed mutagenesis. IE2 induces transactivation of target genes and host cell cycle arrest, and these functions can be selectively abrogated by amino acid substitutions. The H446,452L mutation in a putative zinc finger domain abolishes both DNA binding and host cell cycle arrest abilities (17–19), and the Q548R mutation, which adds a positively charged residue in close proximity to the acidic activation domain, disrupts only the latter (20) (Fig. 4A). The mutant IE2 genes were expressed at levels comparable to those of wild-type IE2 in target cells as assessed by Western blotting (Fig. 4B). Changes in host cell cycle-inhibiting and DNA binding activities of IE2 by the mutations were then tested by quantitative real-time PCR (qPCR) to detect expression of cell cycle inhibitor genes, cdkn1a (p21) (21) and cdkn1b (p27) (22), in the mouse neural progenitor cells (Fig. 4D) and a chromatin immunoprecipitation (ChIP) assay to test IE2 binding to the

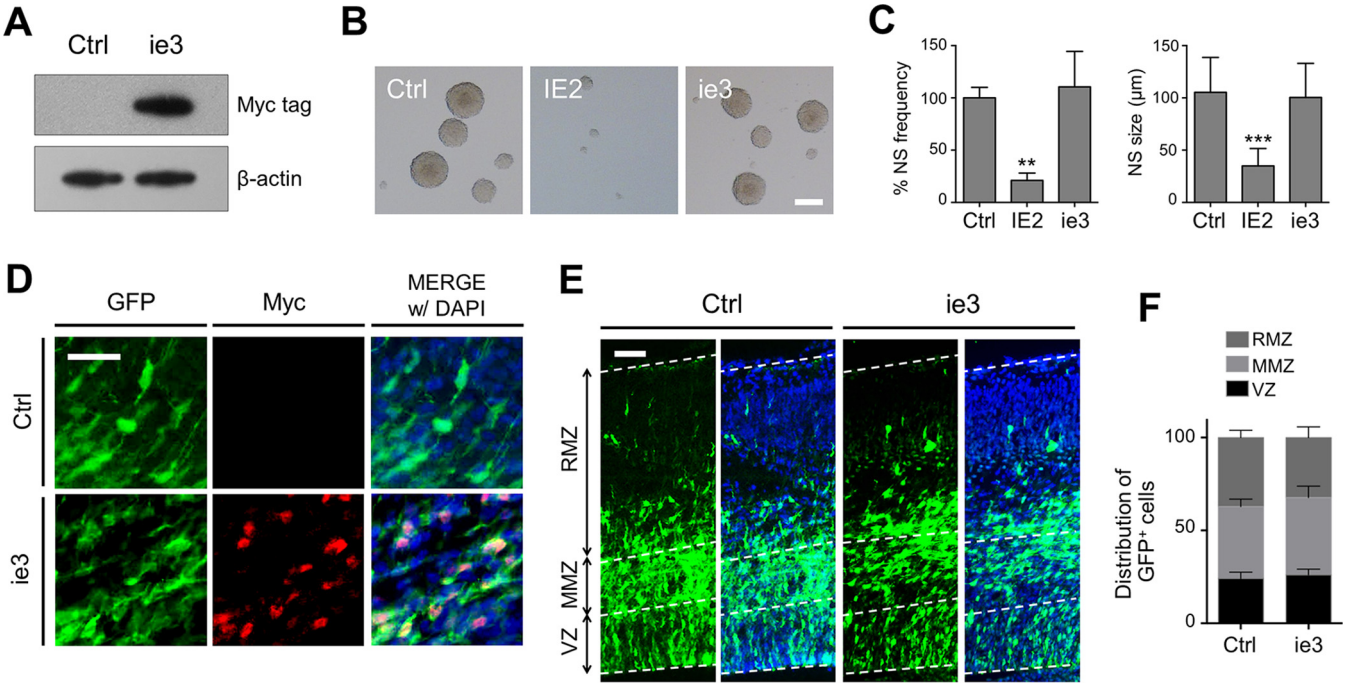

FIG 3 Effects of MCMV ie3 expression on neural stem cell regulation. (A) Expression of Myc-tagged MCMV ie3 in retrovirally transduced embryonic neural progenitors was confirmed by Western blotting using an anti-Myc tag antibody. (B) E14.5 primary neural progenitors transduced with a retroviral vector expressing either HCMV IE2 or MCMV ie3 were cultured for 7 days in neural stem cell medium for neurosphere formation. (C) Quantification of neurosphere frequency and size in of cells shown in panel B. (D) MCMV ie3 expression in the brains at 2 days postelectroporation was examined using anti-GFP (green) and anti-Myc tag (red) primary antibodies and Alexa Fluor 488- and 555-conjugated secondary antibodies. (E) MCMV ie3-expressing cells in E15.5 embryonic brains that were electroporated at E13.5 were immunostained using anti-GFP primary and Alexa Fluor 488-conjugated secondary antibodies. DAPI-merged images are shown on the right. (F) Quantification of GFP$^+$ cell positions of cells shown in panel E. Scale bars were 25 μm (D), 50 μm (E), and 100 μm (B). **, $P < 0.01$; ***, $P < 0.001$; $n \geq 3$.

c-myc promoter region using chromatin extracts derived from mouse neuroblastoma Neuro-2a cells (Fig. 4E).

Upon transduction into primary neural progenitor cells, the Q548R mutation restored neurosphere frequency as well as neurosphere size to 50% of the wild-type IE2 level (Fig. 3F and G), suggesting that the reduced level of *in vitro* stem cell properties induced by IE2 expression is partly attributable to cell cycle inhibition. The DNA binding activity of IE2 appeared to account for the remaining portion of the inhibitory effects of IE2 on neurosphere formation, since the H446,452L mutation almost completely abolished the ability of IE2 to reduce neurosphere frequency and size. These results indicate that the IE2 cell cycle inhibition and DNA binding activities comparably contribute to IE2-induced reduction of neural progenitor cell stemness *in vitro*.

IE2 cell cycle inhibition and DNA binding abilities are responsible for accelerated cell exit from the VZ and mingled neuronal cell polarity *in vivo*, respectively. Finally, we examined the functional consequences of the IE2 mutations *in vivo* by *in utero* electroporation. The reduced fraction of cells in the VZ upon IE2 expression was restored to normal levels by both the Q548R and H446,452L mutations, suggesting that the cell cycle-arresting activity of IE2 is sufficient to cause enhanced neuronal differentiation initiation (Fig. 5A and B). However, IE2 Q548R still produced fewer cells in the upper region of the brain (Fig. 5A and B) and also more nonradial or multipolar cells at the transition between MMZ and RMZ (Fig. 5C and D). Further abrogation of IE2 DNA binding ability was required to rescue the neuronal cell migration, polarization, and migration angle defects. These results indicate that IE2 disrupts normal brain development in a stepwise manner by enhancing neural stem cell exit from the VZ and inhibiting proper polarization of migrating immature neurons, and these are distinctly associated with different IE2 functions, cell cycle-inhibitory and DNA binding (presumably transcriptional regulatory) activities, respectively (Fig. 5E).

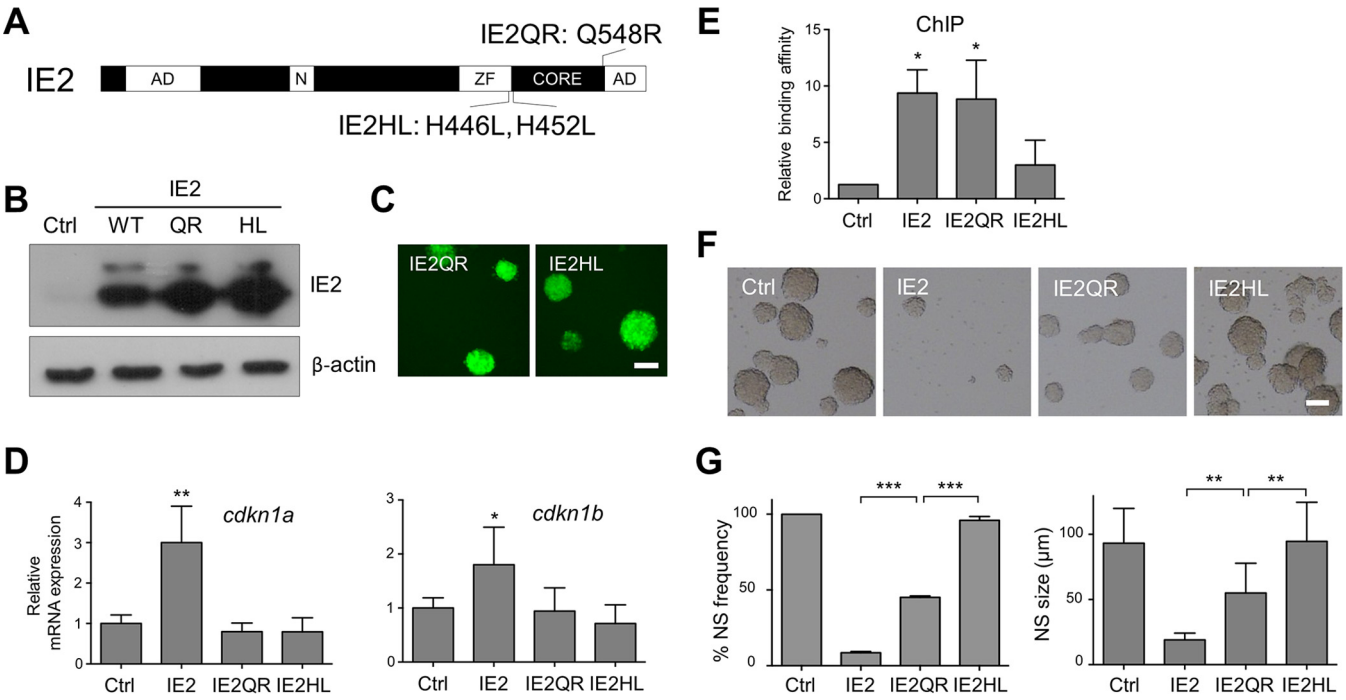

FIG 4 Effects of IE2 mutations on IE2-induced downregulation of neural stem cell properties *in vitro*. (A) Schematic diagram showing the location of the H446,452L and Q548R mutations in the IE2 gene. AD, activation domain; CORE, core domain; N, nuclear localization signal; ZF, putative zinc finger motif. Expression of IE2 mutants and GFP in transduced target cells was confirmed by Western blotting using an anti-IE antibody (B) and fluorescence microscopy (C). (D) Two days after E14.5 primary neural progenitor cells were transduced with each retroviral vector, mRNA expression levels of the indicated cell cycle inhibitor genes were measured by qPCR. (E) Chromatin immunoprecipitation (ChIP) assay using Neuro-2a (a murine neuroblastoma cell line) chromatin extracts and anti-Myc tag antibody and subsequent qPCR analysis for the genomic c-fos promoter region. (F) Effect of IE2 mutants on neurosphere frequency and size. E14.5 primary neural progenitors transduced with the retroviral vectors were cultured for 7 days in serum-free medium supplemented with B27/N2 and FGF2. (G) Quantification of results depicted in panel F. Scale bars, 100 μm. Error bars represent SD. Student's *t* test was used to determine statistical significance. *, $P < 0.05$; **, $P < 0.01$; ***, $P < 0.001$; $n \geq 3$.

DISCUSSION

Stem cells are defined by their ability to produce stem cell progeny, a property known as self-renewal, and their ability to give rise to differentiated cells (23). The self-renewal ability of neural stem cells is important for maintaining neural stem cell pools throughout brain development. Thus, defects in neural stem cell division at early embryonic stages cause depletion of the neural stem cell population, resulting in the failure to produce a proper number and composition of neural cells and subsequently cause microcephaly, a neurodevelopmental disorder characterized by a dramatically smaller brain size at postnatal stages (24). In this regard, it is highly plausible that the ability of IE2 to increase cell cycle exit of neural stem cells would sufficiently address the issue of how HCMV infection can severely reduce brain size or damage brain structures even without viral cytolytic activity.

Proper cortical development requires tightly regulated cell migratory events to establish specific laminar position and connectivity of neurons (25, 26). Most neocortical projection neurons originate by asymmetric division of neural stem cells in the ventricular zone (27). They then move radially to the SVZ and lower IZ, where they become multipolar cells possessing multiple long projections (28, 29). Axon formation starts as cells approach the middle of the IZ, and in the upper part of the IZ, cell morphology changes from multipolar to bipolar cells with a thick, radially oriented leading process and a thin, trailing axon. This polarization of axon and dendrites confers the ability of neurons to migrate to their final destination and communicate with neighboring neurons (30), and errors in neuronal migration are subject to neurodevelopmental disorders, including lissencephaly and focal cortical dysgenesis (31). In this study, we showed that migration of IE2-expressing cells to the cortical plate was greatly delayed, consistent with a previous study reporting delayed migration of bromode-

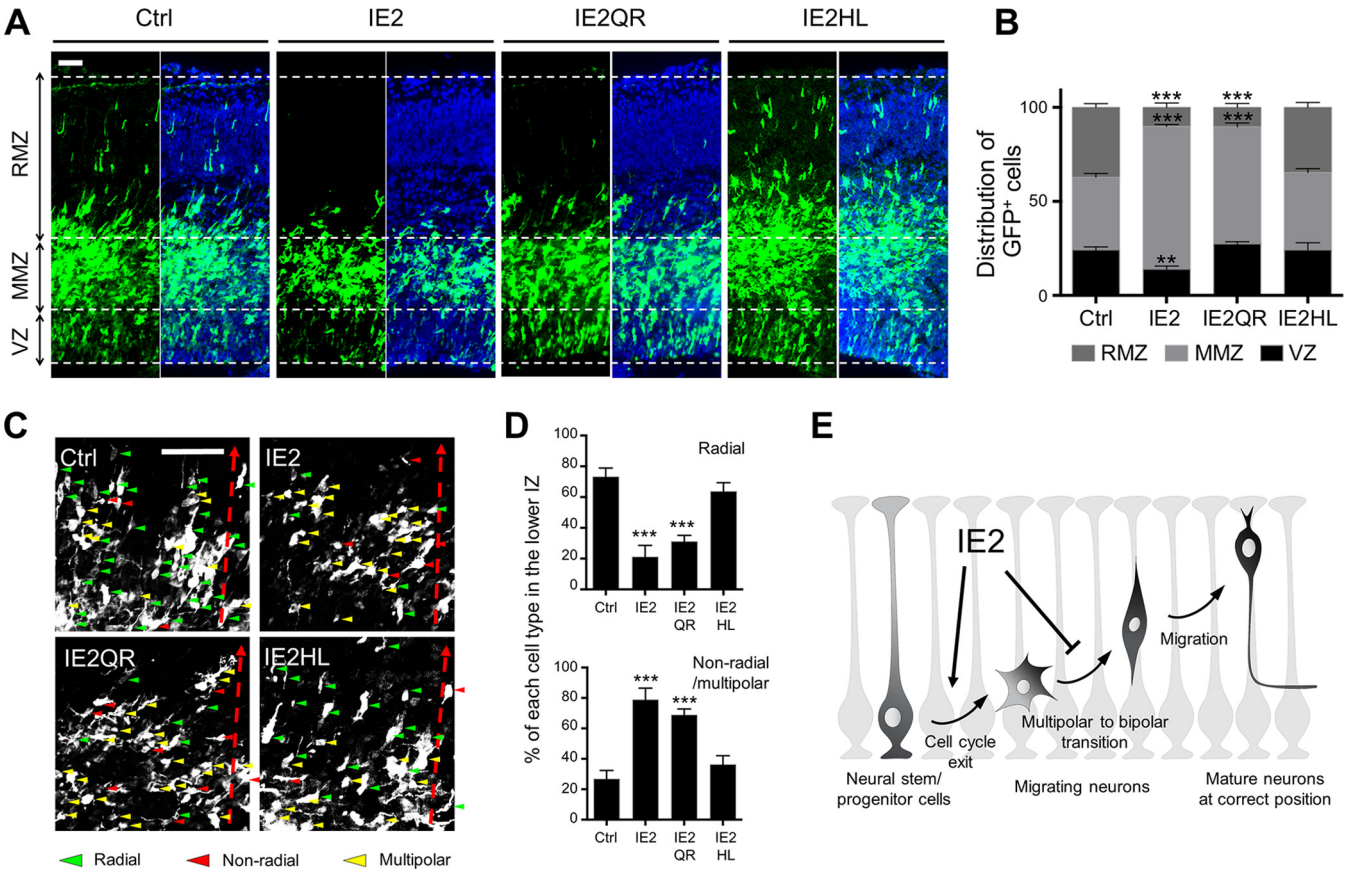

FIG 5 Effects of IE2 mutations on IE2-induced misregulation of neuronal differentiation *in vivo*. (A) Wild-type or mutant IE2-expressing cells in E15.5 embryonic brains that were intraventricularly electroporated at E13.5 were immunolabeled using anti-GFP primary and Alexa Fluor 488-conjugated secondary antibodies. DAPI-merged images are shown on the right. (B) Quantification of GFP$^+$ cell positions shown in panel A. (C) The shapes of cells electroporated with the indicated plasmids in E15.5 cortices at the transition between MMZ and RMZ. The dotted red lines indicate the direction of radial migration. (D) Quantification of GFP$^+$ cell shapes shown in panel C. (E) Schematic representation of a model for the detrimental effects of IE2 on brain development. Expression of IE2 in neural stem cells in the VZ induces the accumulation of nonfunctional immature neurons by enhancing cell cycle exit of neural stem cells and inhibiting multipolar-to-bipolar transition of postmitotic migrating neurons. VZ, ventricular zone; MMZ, multipolar morphology zone; RMZ, radial morphology zone. Scale bars, 50 μm. Error bars represent SD. Student's *t* test was used to determine statistical significance. **, $P < 0.01$; ***, $P < 0.001$; $n \geq 3$.

oxyuridine (BrdU)-labeled cells in postnatal mice infected with MCMV at E15.5 (11). Our careful examination of cell morphology further revealed that the majority of IE2-expressing cells remained as multipolar cells in the boundary region between MMZ and RMZ, where multipolar-to-bipolar transition occurs. Because of the tight functional association between polarization and radial migration of postmitotic neurons (25, 32, 33), we assumed that the lack of IE2-expressing cells in the cortical plate area was due to a defect in the multipolar-to-bipolar transition of migrating neurons, and these defects might also contribute to HCMV-caused neurodevelopmental disorders.

One of the major novel findings of this study is that callosal neurons expressing IE2 were not able to project axons across the midline. Orderly callosal axon projections connecting the two brain hemispheres are critical for coordinated somatosensory and motor functions as well as for higher cognitive processes (34, 35). Consequently, callosal malformations are associated with various types of cognitive, behavioral, and neurological deficits (36). Thus, our data showing impairment of callosal axon projection into the contralateral cortical area offers another possible explanation for brain pathogenesis associated with congenital HCMV infection.

Our sophisticated *in vivo* approaches produced interestingly different conclusions from previous reports employing *in vitro* techniques. For example, HCMV infection was shown to prevent the induction of neuronal differentiation of cultured neural progenitor cells by antineuronal marker immunostaining of cultured cells (37), whereas we

conclude that increased initiation of neuronal differentiation of neural stem cells and inhibition of full neuronal maturation with proper morphology in the correct cortical laminar position may be the real causal mechanism of HCMV neuropathogenesis. They also raised the possibility that late HCMV gene products were responsible for inhibition of neuronal differentiation by using foscarnet sodium (Foscavir), a selective inhibitor of late HCMV gene transcription, whereas we showed that immediate-early protein IE2 has a great impact on neural stem cell differentiation. Although the results are not directly comparable due to different experimental settings (neural progenitor cells *in vitro* versus neural stem cells *in vivo*; HCMV whole virus versus single gene; pharmacological versus direct gain-of-function approach), our *in vivo* approach, which dissects the harmful effects of IE2 on multiple steps of brain development, has meaningful advantages over previous *in vitro* studies.

In summary, our study provides a multistep model for IE2-induced disturbance of brain development. We show that IE2 expression causes enhanced premature cell cycle exit of neural stem cells in the VZ, which can lead to reduction of neural stem cells and a small brain at postnatal stages, followed by inhibition of multipolar-to-bipolar transition and radial migration of new-born neurons which would result in abnormal laminar structures and disruption of connectivity between neurons. It is of note that the broad spectrum of neurodevelopmental disorders caused by HCMV that range from physiological to structural defects can be explained by IE2 action alone. Our characterization of IE2-induced misregulation of neural stem cell maintenance and differentiation provides insight into the role of an individual viral gene in HCMV pathogenesis and furthers our molecular understanding of HCMV-induced developmental CNS disorders.

MATERIALS AND METHODS

Plasmid construction. MSIG-IE1 and -IE2 and MCMV ie3 plasmids were kindly provided by S. Kim (Seoul National University, Seoul, South Korea) and Q. Tang (Howard University College of Medicine, Washington, DC, USA), respectively. The IE2 Q548R and H446,452L mutants were generated by site-directed mutagenesis using the following primers: Q548R (5′-CCGCGAAGGCCTACGCCGTGGGGCGGTTT GAGAAGCCCACCG-3′), H446,452L (5′-CCACTCCCTTCCTCATGGAGCTGACTATGCCTGTGACACTGCCTCCTG ATGTGGCGCAGCG-3′), and the complementary reverse primers. The intended mutations were verified by conventional sequencing. The MCMV ie3 gene was amplified using the ie3-myc tag-F (5′-TCACGCGTGC CACCATGGAACAAAAACTCATCTCAGAAGAGGATCTGAGTTGCAACATGATCATGATCG-3′) and ie3-R (5′-ATGGA TCCTCACTCGCAGTCAGACTCATA-3′) primers and then inserted into the MSIG multicloning site.

Retrovirus preparation and transduction. The method of retroviral vector production was described previously (38). Briefly, the retroviral construct was transfected into 293T cells with gag-pol (pCA-gag-pol) and env-expressing vector (vesicular stomatitis virus glycoprotein) using polyethyleneimine (Sigma). The supernatant was collected 48 h after transfection, filtered through a 0.45-μm filter, and frozen at −80°C until used. Concentrated viral stocks were prepared by ultracentrifugation at 25,000 rpm for 90 min at 4°C in an SW28 rotor (Beckman Coulter). Pellets were resuspended in 50 μl of phosphate-buffered saline (PBS) at 4°C for about 12 h, and virus aliquots were stored at −80°C. For viral titration, NIH 3T3 cells were seeded at 1×10^5 in 6-well plates on the previous day. Viral supernatants were added in the presence of Polybrene (final concentration, 8 μg/ml) (Sigma). Viral titer was determined by measuring the percentage of GFP-positive cells transduced with different dilutions of virus stock.

Animals and *in utero* gene transfer. All animal protocols were approved by the Institutional Review Board (no. SKKUIACUC-2016-04-0005-2) and conducted in the Laboratory Animal Research Center of Sungkyunkwan University. Timed pregnant CD1 mice (Orient Bio) were used for injections, and embryos were considered 0.5 days old (E0.5) when a vaginal plug was detected in the morning. Prior to injection, pregnant mice were anesthetized with pentobarbital sodium (Hanlim Pharm). For *in utero* electroporation, 1 to 2 μl of DNA solution (2 μg/μl) in PBS with 0.01% fast green dye (Sigma) was injected into the lateral ventricle of E13.5 embryos, and five square electric pulses (33 V) were delivered at one pulse per second (50-ms pulse followed by 950-ms gap) to the embryos through the uterus with forceps-type electrodes (CUY650P5; 5-mm-diameter platinum round plates; Nepagene).

Neural progenitor cell preparation and neurosphere assay. Primary neural progenitor cells were prepared from the lateral and medial ganglionic eminences of E14.5 embryos. Dissected brain tissue was minced, washed three times with PBS, and incubated in 0.25% trypsin (Invitrogen) at 37°C for 5 min. DNase and ovomucoid trypsin inhibitor (both from Worthington) were added, and samples were triturated using a fire-polished Pasteur pipette. Cells were washed twice with DMEM–F12 medium (Invitrogen), resuspended in PBS, and run through a 40-μm cell strainer (Falcon). Prior to neurosphere assays, neural progenitors were transduced with concentrated retroviral vectors. After 48 h, aggregated cells were mechanically dissociated, and 3,000 cells were seeded and incubated in DMEM–F12 medium supplemented with B27/N2 (both from Invitrogen) and FGF2 (Peprotech). After 7 days of incubation, the numbers of neurospheres were counted under a light microscope (Eclipse TS100; Nikon).

Immunofluorescence. Standard immunofluorescence procedures were used for visualization of target gene expression in electroporated animals. Briefly, gene-transferred embryonic brains were fixed in 4% paraformaldehyde, dehydrated in 30% sucrose, and cryosectioned. Sections were washed in PBS and then blocked for 1 h with PBS containing 10% fetal bovine serum and 0.2% Triton X-100. Samples were then incubated overnight at 4°C with anti-GFP (1:1,000; Invitrogen) and anti-Sox2 (1:1,000; Chemicon) primary antibodies, washed three times in PBS, and incubated for 3 h at room temperature with Alexa Fluor 488- or 555-conjugated secondary antibodies (Invitrogen) diluted in blocking solution. Samples were further counterstained with 4′,6-diamidino-2-phenylindole (DAPI) (Sigma). Images were acquired using a Zeiss LSM 700 confocal microscope.

Western blotting. Primary neural stem cells were lysed using radioimmunoprecipitation assay (RIPA) buffer (Sigma) with a protease and phosphatase inhibitor cocktail (Pierce Biotechnology). Equal amounts of protein (20 to 40 μg, depending on the target protein) were resolved in 8 to 10% (wt/vol) SDS-PAGE and transferred to polyvinylidene fluoride (PVDF) membranes (PALL). The membranes were blocked with TBST (150 mM NaCl, 10 mM Tris-HCl, 0.1% [vol/vol] Tween 20, pH 8.0) containing 5% (wt/vol) skim milk and analyzed with the following primary antibodies: anti-IE1/2 (1:2,000), anti-cleaved caspase-3 (1:400), anti-Myc tag (1:1,000), and anti-beta-actin (1:2,000). All blots were incubated overnight with a primary antibody at 4°C and with horseradish peroxidase-conjugated anti-mouse or anti-rabbit secondary antibodies (1:10,000; Pierce Biotechnology) for 2 h at room temperature. The protein bands were visualized with the enhanced chemiluminescence system (Atto) and X-Omat film (Kodak).

Reverse transcription and quantitative real-time PCR. Total RNA was prepared from cultured cells using TRIzol reagent (Qiagen), and cDNAs were synthesized from 400 ng of each RNA sample by using an oligo(dT) primer and MMLV-RT enzyme (Promega). Quantitative real-time PCR (qPCR) was performed using the TaKaRa thermal cycler Dice real-time system TP800 (TaKaRa) according to the SmartCycler System's protocol (TaKaRa) with the following primers: cdkn1a-F (5′-CCTGGTG-ATGTCCGACCTG-3′), cdkn1a-R (5′-GCCATGAGCGCATCGCAATCA-3′), cdkn1b-F (5′-TCAAACGTGAGAGTGTCTAACG-3′), cdkn1b-R (5′-CGGGCCGAAGAGATTTCTG-3′), b-actin-F (5′-CAAAAGCCACCCCCACTCCTAAGA-3′), and b-actin-R (5′-GCCCTGGCTGCCTCAACACCTC-3′). All qPCRs were performed by predenaturing at 95°C for 30 s, followed by 43 cycles of three-step amplification at 95°C for 5 s, 60°C for 10 s, and 72°C for 30 s, and a final cycle at 95°C for 15 s, 60°C for 30 s, and 95°C for 15 s, irrespective of target genes.

ChIP. Transfected Neuro2A cells were cross-linked using 1% formaldehyde for 15 min. The samples were then washed three times in cold PBS and homogenized in ChIP cell lysis buffer (1% SDS, 10 mM EDTA, 50 mM Tris-HCl [pH 8.0], and protease inhibitor cocktail [Sigma]). After 10 min on ice, the lysate was sonicated (Cole-Parmer) on ice using 14 pulses of 10 s each at 4 to 6 W and centrifuged for 20 min at 21,000 $\times$ *g* at 4°C, and then the supernatant was collected. An antibody against the Myc tag (1:300; Santa Cruz Biotechnology) was added, and the samples were rotated overnight at 4°C. Immunoprecipitates were isolated by incubating with protein G-agarose (Invitrogen), and the beads were washed consecutively with low-salt buffer (0.1% SDS, 1% Triton X-100, 2 mM EDTA, 20 mM Tris-HCl [pH 8.0], 150 mM NaCl), high-salt buffer (0.1% SDS, 1% Triton X-100, 2 mM EDTA, 20 mM Tris-HCl [pH 8.0], 500 mM NaCl), LiCl buffer (0.25 M LiCl, 1% NP-40, 1% deoxycholic acid, 1 mM EDTA, 20 mM Tris-HCl [pH 8.0]), and TE buffer (1 mM EDTA, 10 mM Tris-HCl [pH 8.0]). Chromatin was eluted and cross-linking was reversed with 0.2 M NaCl. Samples were then digested with 10 μg of proteinase K (Sigma), and DNA was isolated via a DNA purification kit (GeneAll). Enrichment of genomic c-fos promoter regions was determined by qPCR using the c-fosP-F (5′-CAGTGACGTAGGAAGTCCA T-3′) and c-fosP-R (5′-TGCTCGCTGCAGTCGCG-3′) primers.

ACKNOWLEDGMENTS

We thank Sunyoung Kim at Seoul National University, South Korea, for providing the IE1 and IE2 gene plasmids and Qiyi Tang at Howard University College of Medicine for the MCMV ie3 plasmid.

This research was supported by the Basic Science Research Program through the National Research Foundation of Korea (NRF), funded by the Ministry of Science, ICT and Future Planning (2015R1A2A2A01005687).

REFERENCES

1. Griffiths P, Baraniak I, Reeves M. 2015. The pathogenesis of human cytomegalovirus. J Pathol 235:288–297. https://doi.org/10.1002/path.4437.
2. Demmler GJ. 1991. Infectious Diseases Society of America and Centers for Disease Control: summary of a workshop on surveillance for congenital cytomegalovirus disease. Rev Infect Dis 13:315–329. https://doi.org/10.1093/clinids/13.2.315.
3. Grosse SD, Ross DS, Dollard SC. 2008. Congenital cytomegalovirus (CMV) infection as a cause of permanent bilateral hearing loss: a quantitative assessment. J Clin Virol 41:57–62. https://doi.org/10.1016/j.jcv.2007.09.004.
4. Ross SA, Boppana SB. 2005. Congenital cytomegalovirus infection: outcome and diagnosis. Semin Pediatr Infect Dis 16:44–49. https://doi.org/10.1053/j.spid.2004.09.011.
5. Barkovich AJ, Lindan CE. 1994. Congenital cytomegalovirus infection of the brain: imaging analysis and embryologic considerations. Am J Neuroradiol 15:703–715.
6. Koontz T, Bralic M, Tomac J, Pernjak-Pugel E, Bantug G, Jonjic S, Britt WJ. 2008. Altered development of the brain after focal herpesvirus infection of the central nervous system. J Exp Med 205:423–435. https://doi.org/10.1084/jem.20071489.
7. Greig LC, Woodworth MB, Galazo MJ, Padmanabhan H, Macklis JD. 2013. Molecular logic of neocortical projection neuron specification, development and diversity. Nat Rev Neurosci 14:755–769. https://doi.org/10.1038/nrn3586.
8. Hu WF, Chahrour MH, Walsh CA. 2014. The diverse genetic landscape of neurodevelopmental disorders. Annu Rev Genomics Hum Genet 15:195–213. https://doi.org/10.1146/annurev-genom-090413-025600.
9. Compton T, Feire A. 2007. Early events in human cytomegalovirus

infection, p 231–240. *In* Arvin A, Campadelli-Fiume G, Mocarski E, Moore PS, Roizman B, Whitley R, Yamanishi K (ed). Human herpesviruses: biology, therapy, and immunoprophylaxis. Cambridge University Press, Cambridge, United Kingdom.
10. Shinmura Y, Aiba-Masago S, Kosugi I, Li RY, Baba S, Tsutsui Y. 1997. Differential expression of the immediate-early and early antigens in neuronal and glial cells of developing mouse brains infected with murine cytomegalovirus. Am J Pathol 151:1331–1340.
11. Mutnal MB, Cheeran MCJ, Hu S, Lokensgard JR. 2011. Murine cytomegalovirus infection of neural stem cells alters neurogenesis in the developing brain. PLoS One 6:e16211. https://doi.org/10.1371/journal.pone.0016211.
12. Dorsch-Häsler K, Keil GM, Weber F, Jasin M, Schaffner W, Koszinowski UH. 1985. A long and complex enhancer activates transcription of the gene coding for the highly abundant immediate early mRNA in murine cytomegalovirus. Proc Natl Acad Sci U S A 82:8325–8329. https://doi.org/10.1073/pnas.82.24.8325.
13. Jang J, Byun S-H, Han D, Lee J, Kim J, Lee N, Kim I, Park S, Ha S, Kwon M, Ahn J, Chung W-J, Kweon D-H, Cho JY, Kim S, Yoon K. 2014. Notch intracellular domain deficiency in nuclear localization activity retains the ability to enhance neural stem cell character and block neurogenesis in mammalian brain development. Stem Cells Dev 23:2841–2850. https://doi.org/10.1089/scd.2014.0031.
14. Singec I, Knoth R, Meyer RP, Maciaczyk J, Volk B, Nikkhah G, Frotscher M, Snyder EY. 2006. Defining the actual sensitivity and specificity of the neurosphere assay in stem cell biology. Nat Methods 3:801–806. https://doi.org/10.1038/nmeth926.
15. Zhou J, Wen Y, She L, Sui Y-N, Liu L, Richards LJ, Poo M-M. 2013. Axon position within the corpus callosum determines contralateral cortical projection. Proc Natl Acad Sci U S A 110:E2714–E2723. https://doi.org/10.1073/pnas.1310233110.
16. Messerle M, Bühler B, Keil GM, Koszinowski UH. 1992. Structural organization, expression, and functional characterization of the murine cytomegalovirus immediate-early gene 3. J Virol 66:27–36.
17. Macias MP, Stinski MF. 1993. An in vitro system for human cytomegalovirus immediate early 2 protein (IE2)-mediated site-dependent repression of transcription and direct binding of IE2 to the major immediate early promoter. Proc Natl Acad Sci U S A 90:707–711. https://doi.org/10.1073/pnas.90.2.707.
18. Murphy EA, Streblow DN, Nelson JA, Stinski MF. 2000. The human cytomegalovirus IE86 protein can block cell cycle progression after inducing transition into the S phase of permissive cells. J Virol 74:7108–7118. https://doi.org/10.1128/JVI.74.15.7108-7118.2000.
19. Asmar J, Wiebusch L, Truss M, Hagemeier C. 2004. The putative zinc finger of the human cytomegalovirus IE2 86-kilodalton protein is dispensable for DNA binding and autorepression, thereby demarcating a concise core domain in the C terminus of the protein. J Virol 78:11853–11864. https://doi.org/10.1128/JVI.78.21.11853-11864.2004.
20. Petrik DT, Schmitt KP, Stinski MF. 2006. Inhibition of cellular DNA synthesis by the human cytomegalovirus IE86 protein is necessary for efficient virus replication. J Virol 80:3872–3883. https://doi.org/10.1128/JVI.80.8.3872-3883.2006.
21. Harper JW, Adami GR, Wei N, Keyomarsi K, Elledge SJ. 1993. The p21 Cdk-interacting protein Cip1 is a potent inhibitor of G1 cyclin-dependent kinases. Cell 75:805–816. https://doi.org/10.1016/0092-8674(93)90499-G.
22. Polyak K, Lee M-H, Erdjument-Bromage H, Koff A, Roberts JM, Tempst P, Massagué J. 1994. Cloning of p27Kip1, a cyclin-dependent kinase inhibitor and a potential mediator of extracellular antimitogenic signals. Cell 78:59–66. https://doi.org/10.1016/0092-8674(94)90572-X.
23. Morrison SJ, Kimble J. 2006. Asymmetric and symmetric stem-cell divisions in development and cancer. Nature 441:1068–1074. https://doi.org/10.1038/nature04956.
24. Bond J, Woods CG. 2006. Cytoskeletal genes regulating brain size. Curr Opin Cell Biol 18:95–101. https://doi.org/10.1016/j.ceb.2005.11.004.
25. Kriegstein AR, Noctor SC. 2004. Patterns of neuronal migration in the embryonic cortex. Trends Neurosci 27:392–399. https://doi.org/10.1016/j.tins.2004.05.001.
26. Rakic P. 2007. The radial edifice of cortical architecture: from neuronal silhouettes to genetic engineering. Brain Res Rev 55:204–219. https://doi.org/10.1016/j.brainresrev.2007.02.010.
27. Jossin Y, Cooper JA. 2011. Reelin, Rap1 and N-cadherin orient the migration of multipolar neurons in the developing neocortex. Nat Neurosci 14:697–703. https://doi.org/10.1038/nn.2816.
28. Bielas S, Higginbotham H, Koizumi H, Tanaka T, Gleeson JG. 2004. Cortical neuronal migration mutants suggest separate but intersecting pathways. Annu Rev Cell Dev Biol 20:593–618. https://doi.org/10.1146/annurev.cellbio.20.082503.103047.
29. Noctor SC, Martínez-Cerdeño V, Ivic L, Kriegstein AR. 2004. Cortical neurons arise in symmetric and asymmetric division zones and migrate through specific phases. Nat Neurosci 7:136–144.
30. Barnes AP, Polleux F. 2009. Establishment of axon-dendrite polarity in developing neurons. Annu Rev Neurosci 32:347–381. https://doi.org/10.1146/annurev.neuro.31.060407.125536.
31. Sarkisian MR, Bartley CM, Rakic P. 2008. Trouble making the first move: interpreting arrested neuronal migration in the cerebral cortex. Trends Neurosci 31:54–61. https://doi.org/10.1016/j.tins.2007.11.009.
32. Tabata H, Nakajima K. 2003. Multipolar migration: the third mode of radial neuronal migration in the developing cerebral cortex. J Neurosci 23:9996–10001.
33. LoTurco JJ, Bai J. 2006. The multipolar stage and disruptions in neuronal migration. Trends Neurosci 29:407–413. https://doi.org/10.1016/j.tins.2006.05.006.
34. Gazzaniga MS, Bogen JE, Sperry RW. 1962. Some functional effects of sectioning the cerebral commissures in man. Proc Natl Acad Sci U S A 48:1765–1769.
35. Witelson SF. 1985. The brain connection: the corpus callosum is larger in left-handers. Science 229:665–668.
36. Paul LK, Brown WS, Adolphs R, Tyszka JM, Richards LJ, Mukherjee P, Sherr EH. 2007. Agenesis of the corpus callosum: genetic, developmental and functional aspects of connectivity. Nat Rev Neurosci 8:287–299. https://doi.org/10.1038/nrn2107.
37. Odeberg J, Wolmer N, Falci S, Westgren M, Seiger Å Söderberg-Nauclér C. 2006. Human cytomegalovirus inhibits neuronal differentiation and induces apoptosis in human neural precursor cells. J Virol 80:8929–8939. https://doi.org/10.1128/JVI.00676-06.
38. Lee N, Kim I, Park S, Han D, Ha S, Kwon M, Kim J, Byun S-H, Oh W, Jeon HB, Kweon D-H, Cho JY, Yoon K. 2015. Creatine inhibits adipogenesis by downregulating insulin-induced activation of the phosphatidylinositol 3-kinase signaling pathway. Stem Cells Dev 24:983–994. https://doi.org/10.1089/scd.2014.0130.